Atmospheric Ar and Ne returned from mantle depths to the Earth's surface by forearc recycling

Suzanne L. Baldwin[1] and J. P. Das

Department of Earth Sciences, Syracuse University, Syracuse, NY 13244

Edited by T. Mark Harrison, University of California, Los Angeles, CA, and approved October 9, 2015 (received for review December 16, 2014)

In subduction zones, sediments, hydrothermally altered lithosphere, fluids, and atmospheric gases are transported into the mantle, where ultrahigh-pressure (UHP) metamorphism takes place. However, the extent to which atmospheric noble gases are trapped in minerals crystallized during UHP metamorphism is unknown. We measured Ar and Ne trapped in phengite and omphacite from the youngest known UHP terrane on Earth to determine the composition of Ar and Ne returned from mantle depths to the surface by forearc recycling. An $^{40}Ar/^{39}Ar$ age [7.93 ± 0.10 My (1σ)] for phengite is interpreted as the timing of crystallization at mantle depths and indicates that $^{40}Ar/^{39}Ar$ phengite ages reliably record the timing of UHP metamorphism. Both phengite and omphacite yielded atmospheric $^{38}Ar/^{36}Ar$ and $^{20}Ne/^{22}Ne$. Our study provides the first documentation, to our knowledge, of entrapment of atmospheric Ar and Ne in phengite and omphacite. Results indicate that a subduction barrier for atmospheric-derived noble gases does not exist at mantle depths associated with UHP metamorphism. We show that the crystallization age together with the isotopic composition of nonradiogenic noble gases trapped in minerals formed during subsolidus crystallization at mantle depths can be used to unambiguously assess forearc recycling of atmospheric noble gases. The flux of atmospheric noble gas entering the deep Earth through subduction and returning to the surface cannot be fully realized until the abundances of atmospheric noble gases trapped in exhumed UHP rocks are known.

subduction | UHP metamorphism | geochronology | noble gas | atmosphere

It has long been known that water and CO_2 can be transported into the deep Earth by subduction of sediments and hydrothermally altered oceanic crust (1–3). Water is carried from the surface into the upper mantle by hydrous minerals in the uppermost 10–12 km subducting lithosphere to depths of at least 400 km (4). However, to what extent are atmospheric noble gases transported into the deep Earth and returned to the surface in the forearcs of subduction zones? The isotopic compositions of Ar and Ne can be used as tracers of atmospheric recycling in subduction zones (5), because they are chemically inert at conditions relevant to processes on Earth (6). Serpentinite subduction has been proposed as a viable mechanism for high abundances of noble gas to be transported into the mantle (7), and hydration of oceanic lithosphere has been proposed as a mechanism to release argon into the atmosphere (8). To determine the flux of atmospheric noble gases recycled into the mantle in subduction zones requires knowing when, at what depth, and how atmospheric Ar and Ne are trapped in minerals crystallized at mantle depths and subsequently, exhumed to the surface. This flux calculation requires interpreting noble gas concentrations in minerals with respect to their pressure–temperature–time–deformation (P-T-t-D) histories.

Studies that have addressed recycling of atmospheric noble gases in the Earth's mantle have largely focused on volcanic rocks in arcs, backarcs, ocean island basalts, and midocean ridge basalts (MORBs) (5). However, atmospheric-derived noble gases have been shown to contaminate mantle noble gas signatures in volcanic rocks, irrespective of eruption setting (underwater, under ice, or in atmosphere) (9). Indeed, $^{38}Ar/^{36}Ar$ values for mantle-derived volcanic rocks generally have been found to be indistinguishable from atmospheric ratios (10, 11). The possibility of atmospheric contamination during eruption or interaction with meteoric fluids and seawater exists for any mineral/rock formed, or altered, at or near the Earth's surface.

Noble gas studies of peridotites (12) and serpentinized peridotites (13) have also argued for recycling of atmospheric noble gases into Earth's mantle; however, linking the conditions of noble gas entrapment to specific parts of P-T-t-D histories in these lithologies is challenging. Peridotites are readily altered on the seafloor at temperatures <500 °C, where olivine and orthopyroxene react to form serpentine minerals. Serpentinite forms in many tectonic settings (14) and is stable over a wide range of pressure–temperature conditions (2). High-pressure serpentinites have been used to investigate noble gas and halogen compositions interpreted to have been trapped during subseafloor alteration and subsequent dehydration metamorphism (7). Noble gas and halogen studies of the Higashi-akaishi peridotite body of the Sanbagawa metamorphic terrane argue for the subduction and survival of marine pore fluid to depths of at least 100 km (15). The prograde pressure–temperature–deformation path of the peridotite is not well-constrained, and it is unclear whether early deformation is related to subduction (16). Therefore, several interpretations are possible to explain when and how entrapment of noble gases occurred (e.g., during prograde metamorphism, peak metamorphism, exhumation, or obduction).

This study investigates noble gases, specifically Ar and Ne, trapped in minerals that formed during ultrahigh-pressure (UHP) metamorphism. Exhumed UHP rocks have been shown to preserve a record of the geochemical and fluid transport of material from mantle depths to the Earth's surface (17–19). The forearc subduction channel provides a pathway for "input" lithologies (continental and oceanic crust and sediments) to be recycled, because they are metamorphosed at mantle depths where diagnostic assemblages (e.g., coesite and diamond) can crystallize and trap noble gases during

Significance

The abundance of atmospheric noble gases trapped in the deep Earth has been impacted by the extent to which the Earth's atmosphere is transported into the mantle through subduction processes. However, little is known about the recycling of atmospheric gases in forearcs. We measured Ar and Ne in the world's youngest exhumed coesite eclogite and found that atmospheric Ar and Ne were trapped in phengite and omphacite during crystallization at mantle depths. This Ar and Ne study is the first study, to our knowledge, to document when atmospheric Ar and Ne were trapped in ultrahigh-pressure metamorphic rocks, and it shows that forearc recycling is a viable mechanism for return of atmospheric Ar and Ne to the Earth's surface in rocks exhumed from mantle depths.

Author contributions: S.L.B. and J.P.D. designed research, performed research, analyzed data, and wrote the paper.

The authors declare no conflict of interest.

This article is a PNAS Direct Submission.

[1]To whom correspondence should be addressed. Email: sbaldwin@syr.edu.

This article contains supporting information online at www.pnas.org/lookup/suppl/doi:10.1073/pnas.1424122112/-/DCSupplemental.

UHP metamorphism. When UHP rocks are subsequently returned (exhumed) to the surface, their mineral assemblages provide clues to the changing conditions along their P-T-t-D paths. Thus, noble gases trapped in material entering (in crust and sediments) and exiting (in high-pressure and UHP metamorphic rocks) forearcs can provide insight into the recycling of atmospheric noble gases within the subduction channel. Previous studies that have investigated noble gases in exhumed high-pressure and UHP rocks focused on (*i*) $^{40}Ar/^{39}Ar$ age determination on irradiated K-bearing minerals (20), (*ii*) He and Ne isotopic studies aimed at documenting noble gas compositions trapped during diamond formation (21), and (*iii*) noble gas and halogen studies of serpentinite and peridotite (7, 12, 15). Here, we investigate whether atmospheric Ar and Ne are trapped in minerals during crystallization at mantle depths during subduction zone metamorphism. We present Ar and Ne isotopic data for omphacite and phengite from Late Miocene coesite eclogite that document both the $^{40}Ar/^{39}Ar$ age of phengite crystallization and the isotopic composition of Ar and Ne trapped in these minerals during UHP metamorphism.

Geologic Setting and Sample Description

The coesite eclogite studied (sample 89321) is the youngest known exhumed UHP rock on Earth, and it was sampled from Tomabaguna Island in eastern Papua New Guinea (22). Mafic eclogites are inferred to have originated as dikes that were metamorphosed in situ and now occur as eclogite boudins within strongly folded and isoclinally folded garnet-bearing quartzofeldspathic host gneisses (23–26). Foliation in the mafic eclogites is roughly concordant with that in the host gneiss. The eclogite boudins have retrograde amphibolite rinds. Pegmatite veins (3.52 ± 0.10 Ma) intrude the quartzofeldspathic host and are locally concordant with the gneissic foliation (27). Apatite fission track ages for the coesite eclogite host gneiss (0.6 ± 0.2 Ma) indicate exhumation to shallow crustal levels by the middle Pleistocene (27). Geologic and structural data (25), electron backscatter diffraction measurements, and phase relations (28) provide additional outcrop and regional-scale geochemical (29) and P-T-t-D constraints for the UHP terrane (30). These studies provide the context for interpretation of the coesite eclogite Ar and Ne data presented here.

The coesite eclogite preserves a peak assemblage of garnet + omphacite + rutile + phengite + coesite (Fig. 1*A*). Coesite occurs as an inclusion in omphacite (Fig. 1*B*). In situ U-Pb zircon ion probe analyses of primarily zircon inclusions in garnet yielded a $^{206}Pb/^{238}U$ age of 7.9 ± 1.9 Ma (2σ) on this sample (31). Garnet from this sample also yielded an Lu-Hf isochron age of 7.1 ± 0.7 Ma (2σ) (32). Thermobarometric estimates of crystallization are derived from both mineral assemblages (i.e., garnet, pyroxene, and phengite) and trace element concentrations (zircon and rutile) (23). The combined thermobarometry, geochronology, and geochemical (29) dataset for this sample is interpreted to indicate that a garnet-bearing partial mantle melt intruded subducted metasediments and crystallized at UHP conditions (>90-km depth) to form coesite eclogite. The pressure–temperature conditions of coesite eclogite formation are indicated by the star in Fig. 1*C*. Subsequently, the coesite eclogite was exhumed from mantle depths to the Earth's surface at average rates of ≥1 cm y^{-1} (33).

$^{40}Ar/^{39}Ar$ Age of Phengite from Coesite Eclogite

We first performed an $^{40}Ar/^{39}Ar$ step heat experiment on phengite, a high-silicon variety of muscovite, and the dominant hydrous potassic phase in UHP metamorphic rocks. One objective was to assess whether results could be interpreted within a geologic and tectonic context or yielded anomalously old $^{40}Ar/^{39}Ar$ apparent ages because of incorporation of "excess Ar" [$^{40}Ar/^{36}Ar$ > 298.56 (34)] as

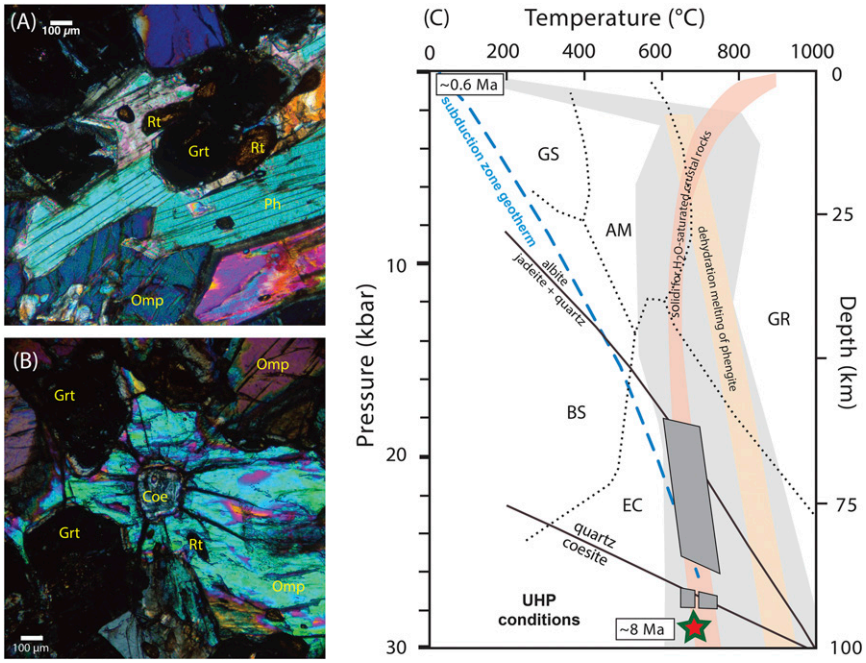

Fig. 1. (*A* and *B*) Photomicrographs of 89321 coesite eclogite from the Papua New Guinea UHP terrane. Cross-polarized light at 10× magnification. Abbreviations are garnet (Grt), omphacite (Omp), phengite (Ph), and rutile (Rt). Coesite (Coe) occurs as an inclusion in omphacite. (*C*) Peak pressure–temperature–time constraints for 89321 coesite eclogite (star). Thermobarometry constraints for coesite eclogite are indicated by dark gray boxes (22). Timing of peak metamorphism based on $^{40}Ar/^{39}Ar$ phengite (this study), Lu-Hf garnet (27), and U-Pb zircon (31) ages. Apatite fission track ages (0.6 Ma) from host gneiss at the coesite locality constrain the timing of exhumation to shallow crustal levels (27). Abbreviations for metamorphic facies are blueschist (BS), greenschist (GS), amphibolite (AM), eclogite (EC), and granulite (GR); mineral abbreviations are albite (Ab), jadeite (Jd), and quartz (Qtz). The light gray path shows the range in pressure–temperature conditions for the UHP terrane (33). The dashed blue line indicates subduction zone geotherm. The solidus for water-saturated crustal rocks and dehydration melting of phengite (36, 52) provide maximum temperature limits for the pressure–temperature–time path followed by coesite eclogite during exhumation to the surface.

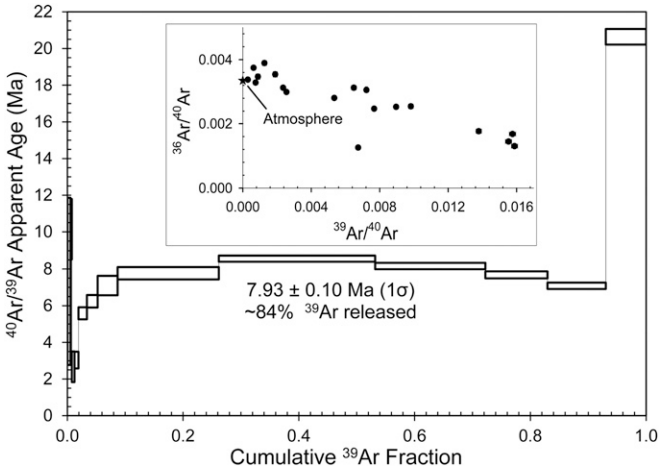

Fig. 2. Results of step heat experiment on phengite from coesite eclogite in the Papua New Guinea UHP terrane. The $^{40}Ar/^{39}Ar$ age spectrum is shown together with the inverse isochron plot (*Inset*). Data corrected for blanks, mass discrimination, and reactor-produced isotopes. Steps used to calculate the weighted mean age correspond to 84% of ^{39}Ar released. The inverse isochron suggests mixing between radiogenic and atmospheric argon components. Additional discussion is in the text.

inferred in some studies of UHP terranes (35). Results of an $^{40}Ar/^{39}Ar$ step heat experiment on phengite yielded an age spectrum characterized by youngest $^{40}Ar/^{39}Ar$ apparent ages of ~2.7 Ma followed by apparent ages that gradually rise over the first ~9% of the gas released to ~8 Ma (Fig. 2 and Table S1). Apparent ages corresponding to 84% of ^{39}Ar released yielded an $^{40}Ar/^{39}Ar$ weighted mean age of 7.93 ± 0.10 Ma (1σ). The highest temperature step (1,600 °C) yielded an $^{40}Ar/^{39}Ar$ apparent age of 20.64 ± 0.90 Ma (1σ) with a corresponding high $^{37}Ar/^{39}Ar$ ratio, and it likely reflects outgassing of retentive high Ca/K inclusion(s) within phengite. We interpret the youngest $^{40}Ar/^{39}Ar$ apparent ages to result from minor neocrystallization on phengite grain boundaries during exhumation, which occurred after crystallization of pegmatitic muscovite at the same outcrop (27). The $^{40}Ar/^{39}Ar$ weighted mean age for phengite based on ~84% of ^{39}Ar released is interpreted to date the time of phengite crystallization. The weighted mean age is concordant with previously published $^{238}U/^{206}Pb$ zircon ages (31) and an Lu-Hf garnet isochron age (32), all obtained on the same sample. The preservation of phengite and its corresponding $^{40}Ar/^{39}Ar$ weighted mean age indicate that the coesite eclogite did not follow a subduction and exhumation path that allowed for the dehydration breakdown of phengite (36). Furthermore, complete outgassing/resetting of radiogenic argon ($^{40}Ar^*$) did not occur during exhumation. Inverse isochron (20) analysis for the phengite step heat experiment yielded a poorly defined mixing array between atmospheric and radiogenic components (Fig. 2, *Inset*). A step heat experiment was also performed on irradiated omphacite. However, its low potassium content (<0.03 wt % K_2O) compared with phengite (8.84–9.91 wt % K_2O) (22) prevented age determination (Table S1).

Fig. 3 shows a comparison of the concentrations of Ar isotopes released as a function of temperature during the step heat experiments on phengite and omphacite. In the case of phengite, a strong correlation exists for the temperature at which (*i*) radiogenic $^{40}Ar^*$ produced from radiogenic decay of ^{40}K, (*ii*) $^{39}Ar_K$ produced during (n,p) irradiation of ^{39}K, (*iii*) $^{38}Ar_{Cl}$ produced by $^{37}Cl(n,\gamma)^{38}Cl(\beta)^{38}Ar$ reaction during irradiation, and (*iv*) stable ^{36}Ar are outgassed. Phengite was retentive to argon loss during laboratory step heating, with >99% of the sample outgassed at temperatures >970 °C (Table S1). The fact that both K- and Cl-derived Ar isotopes as well as stable ^{36}Ar outgas at similar temperatures suggests that Ar is derived from the crystalline lattice in phengite and not from fluid inclusions. This interpretation is also supported by the concordance of $^{40}Ar/^{39}Ar$ ages for >1,200 °C steps with U-Pb zircon (31) and Lu-Hf garnet (32) ages from the same sample. In the case of low [K] omphacite, Ar is outgassed at relatively low temperatures (<1,200 °C), and additional work is required to ascertain whether Ar is trapped in fluid inclusions or within the crystalline lattice.

Ar and Ne in Phengite and Omphacite

We performed additional step heat experiments on (unirradiated) splits of phengite and omphacite to investigate the composition and concentrations of trapped Ar and Ne in minerals crystallized during UHP metamorphism at mantle depths (>90 km). Fig. 4 shows an argon three-isotope plot ($^{40}Ar/^{36}Ar$ vs. $^{38}Ar/^{36}Ar$) for all data

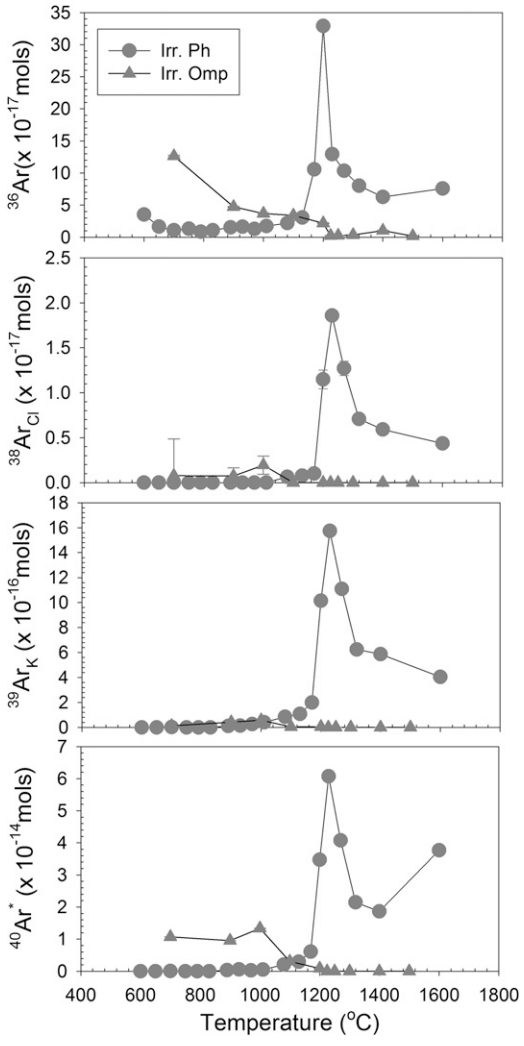

Fig. 3. Argon abundances for irradiated phengite and omphacite from coesite eclogite vs. temperatures (°C) of laboratory outgassing. The comparison of phengite and omphacite values indicates that overall relatively higher abundances of Ar are outgassed from phengite and that most of Ar in phengite was released during laboratory heating at temperatures >1,200 °C. Radiogenic ($^{40}Ar^*$) is produced from radiogenic decay of ^{40}K. $^{39}Ar_K$ is produced during (n,p) irradiation of ^{39}K. $^{38}Ar_{Cl}$ is produced by $^{37}Cl(n,\gamma)^{38}Cl(\beta)^{38}Ar$ reaction during irradiation. ^{36}Ar is the stable isotope of Ar, assumed to be primordial and/or atmospheric-derived. Irr. Ph, irradiated phengite; Irr. Omp, irradiated omphacite.

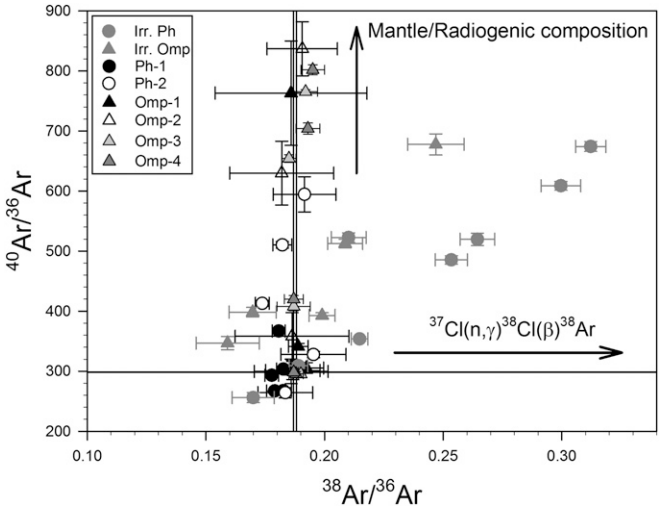

Fig. 4. Argon isotopic compositions for both irradiated and natural (unirradiated) phengite and omphacite from coesite eclogite in the Papua New Guinea UHP terrane. Reference lines for atmospheric compositions ($^{40}Ar/^{36}Ar$ and $^{38}Ar/^{36}Ar$) are indicated (34). Results of step heat experiments on natural samples fall on a mixing line between atmospheric $^{38}Ar/^{36}Ar$ and $^{40}Ar/^{36}Ar$ ratios produced from a mixture of radiogenic and atmospheric components. Data for irradiated samples result from Ar-trapped component mixtures of atmospheric-, radiogenic-, and reactor-produced ^{38}Ar. Errors are 1σ. For irradiated samples, reactor-produced ^{38}Ar shifts $^{38}Ar/^{36}Ar$ ratios to values greater than the atmospheric ratio as indicated. Irr. Ph, irradiated phengite; Irr. Omp, irradiated omphacite; Omp, omphacite; Ph, phengite.

(i.e., results on both irradiated and unirradiated splits of phengite and omphacite) for which the blank contribution was less than 20% for ^{36}Ar (Tables S1 and S2). Atmospheric $^{40}Ar/^{36}Ar$ and $^{38}Ar/^{36}Ar$ reference lines (34) are indicated. Because of the presence of variable amounts of radiogenic $^{40}Ar^*$, results yielded $^{40}Ar/^{36}Ar$ ratios that are generally greater than atmospheric values. However, with few exceptions, the $^{38}Ar/^{36}Ar$ values on natural (unirradiated) phengite and omphacite are within error of atmospheric $^{38}Ar/^{36}Ar$ ratios.

Step heat experiments on irradiated phengite and omphacite yielded $^{38}Ar/^{36}Ar$ ratios above atmospheric values (>0.1885) (Fig. 4). These higher $^{38}Ar/^{36}Ar$ ratios from outgassed irradiated samples result from reactor-produced $^{38}Ar_{Cl}$ [i.e., by the nuclear reaction $^{37}Cl(n,\gamma)^{38}Cl(\beta)^{38}Ar$]. We initially considered, as observed in prior studies of noble gases in fluid inclusions (37), that Cl-derived ^{38}Ar is sourced from fluid inclusions, with the high-temperature release of $^{38}Ar_{Cl}$ being the result of outgassing of smaller (<1–2 μm) fluid inclusions. However, as discussed above, the phengite Ar release patterns (Fig. 3), concordant $^{40}Ar/^{39}Ar$ phengite ages, together with Cl anionic substitution for (OH) in the mica structure (38) suggest that Cl-derived ^{38}Ar is sourced from the crystalline lattice and not from fluid inclusions.

Neon isotopes (^{20}Ne and ^{22}Ne) were used to further constrain the composition of trapped noble gases in phengite and omphacite from coesite eclogite (Fig. 5 and Table S2). Results of step heat experiments are shown on a plot of $^{20}Ne/^{22}Ne$ vs. $^{38}Ar/^{36}Ar$, with atmospheric $^{20}Ne/^{22}Ne$ and $^{38}Ar/^{36}Ar$ reference lines (39) indicated (Fig. 5). Data with large contributions of blank (for Ne >25% and for Ar >20%) are not plotted in Fig. 5. The majority of results plot within (1σ) error of atmospheric values, including for high-temperature steps (>1,400 °C). For comparison, $^{20}Ne/^{22}Ne$ results are within the range of $^{20}Ne/^{22}Ne$ ratios obtained on metamorphic diamonds from the Kokchetav UHP massif of Kazakhstan (21), with the exception of one phengite analysis (Phg-1; 1,500 °C step). No evidence for trapped mantle-derived $^{20}Ne/^{22}Ne$ [either solar or neon B (40, 41)] was obtained, despite mantle εNd and εHf values obtained on garnet from the same coesite eclogite (29).

For most temperature steps, we were not able to determine ^{21}Ne concentrations because of the small signal size relative to blank. In cases where we were able to determine ^{21}Ne concentrations (Table S2), $^{21}Ne/^{22}Ne$ are atmospheric ratios [i.e., 0.029 (39)]. The steps for which we could not determine ^{21}Ne concentration are still consistent with an atmospheric interpretation, because MORB $^{21}Ne/^{22}Ne$ ratios are 0.060 (42) and would have resulted in higher detectable ^{21}Ne concentrations than we observed.

A plot of the $^{20}Ne/^{36}Ar$ elemental ratio vs. $^{38}Ar/^{36}Ar$ for the phengite and omphacite data indicates the data results from mixing between sedimentary, seawater, atmospheric, and MORB components (Fig. 6). However, we caution that, as long as the phase remains stable, the release of Ne and Ar from the crystalline lattices of phengite and omphacite during step heat experiments is controlled by their relative diffusivities. Therefore, reliance on only the $^{20}Ne/^{36}Ar$ elemental ratio may not be sufficient to deconvolve the various contributions.

Adsorbed gas is desorbed under vacuum (43). Because samples were outgassed in a double-vacuum resistance heated furnace connected to an ultrahigh-vacuum line and because K- and Cl-derived argon isotopes and stable ^{36}Ar were all released at high temperatures in the laboratory, the source of ^{36}Ar cannot be adsorbed argon. We can, thus, eliminate the possibility that atmospheric contamination at the surface—in either the field or the laboratory—can explain the results presented. No fluid inclusions were observed in polished thin sections. Furthermore, concordant $^{40}Ar/^{39}Ar$ phengite, Lu-Hf garnet, and U-Pb zircon ages for this sample together with the temperature-dependent Ar release patterns (Fig. 2) suggest that results are not the product of outgassing

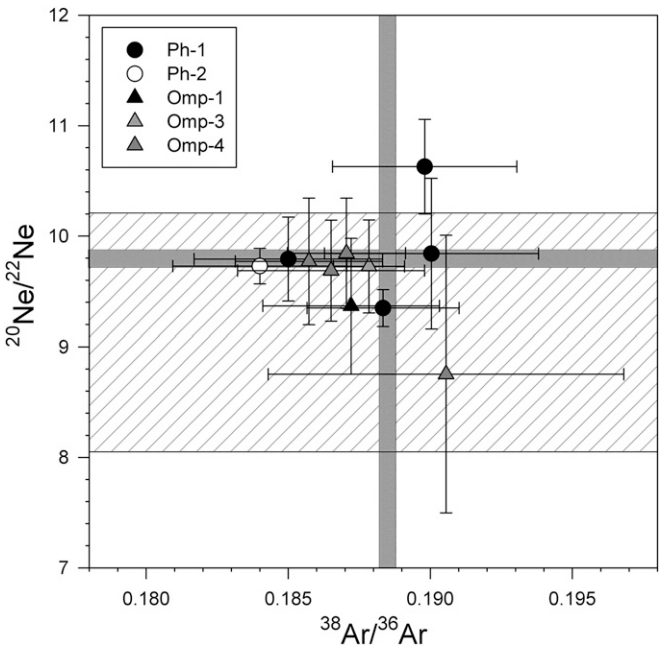

Fig. 5. $^{20}Ne/^{22}Ne$ and $^{38}Ar/^{36}Ar$ isotope data for step heat experiments on unirradiated (natural) omphacite and phengite. Data with large contributions from blank (>20% for Ar and >25% for Ne) are not included. Atmospheric values for $^{20}Ne/^{22}Ne$ and $^{38}Ar/^{36}Ar$ ratios (39) are indicated with horizontal and vertical lines, respectively. Results indicate the presence of trapped neon and argon, with compositions within error of the atmospheric values, in both omphacite and phengite. The hatched area indicates the range of $^{20}Ne/^{22}Ne$ values obtained for metamorphic diamonds from the Kokchetav massif (21). Neither mantle nor solar wind $^{20}Ne/^{22}Ne$ values were observed (44) in phengite and omphacite from the coesite eclogite studied. Omp, omphacite; Ph, phengite.

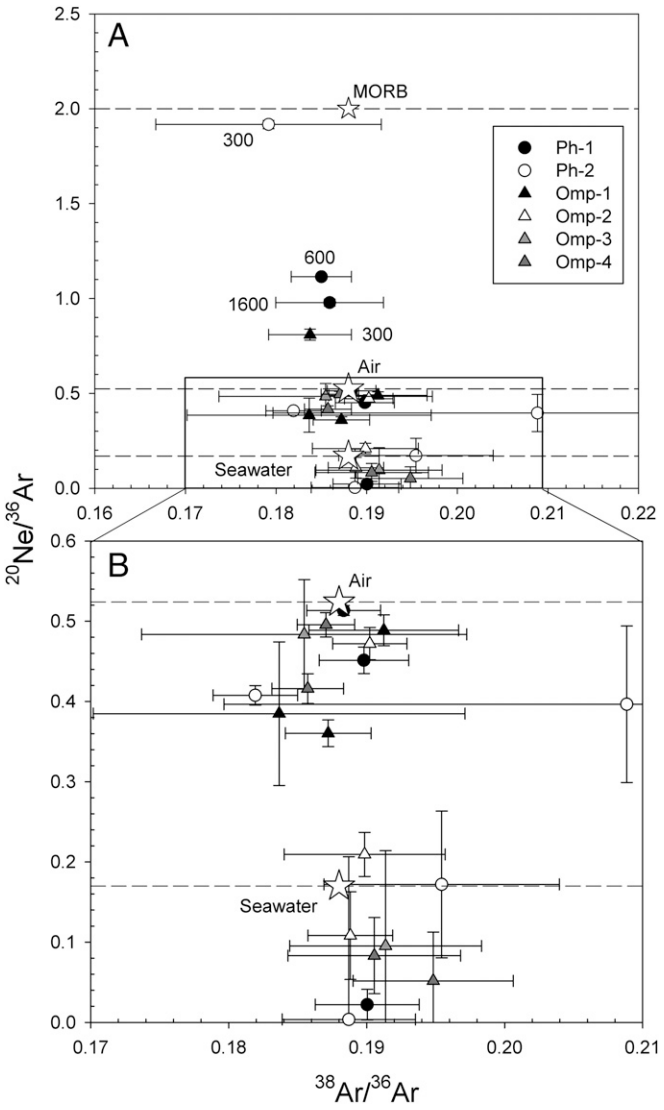

Fig. 6. Plot of $^{20}Ne/^{36}Ar$ vs. $^{38}Ar/^{36}Ar$ for step heat experiments on unirradiated (natural) omphacite and phengite. Stars indicate MORB, air, and seawater values. Horizontal dashed lines indicate $^{20}Ne/^{36}Ar$ values for MORB, air, and seawater. Because the release of trapped Ne and Ar from a mineral at a given temperature is controlled by their relative diffusivities, use of an elemental ratio (i.e., $^{20}Ne/^{36}Ar$) to decipher mixing components from step heat experiments is not always straightforward. (*A*) Four data points (two from phengite-1 and one each from phengite-2 and omphacite-1) have $^{20}Ne/^{36}Ar$ values between atmospheric and MORB values. Numbers other than these data points indicate extraction temperature (degrees Celsius). We did not detect ^{22}Ne in three of the steps because of higher contribution of blank and/or higher analytical error. For the 600 °C extraction step for the phengite-1 sample, the $^{20}Ne/^{22}Ne$ is atmospheric, despite $^{20}Ne/^{36}Ar$ indicating the presence of an MORB component. (*B*) An enlarged section of *A*, with data showing $^{20}Ne/^{36}Ar$ ratios that range between atmospheric and seawater values. Lowest values (0.003) may derive from contributions from a sedimentary component (ref. 7 and references therein). Omp, omphacite; Ph, phengite.

of fluid inclusions in the laboratory. We, therefore, interpret the data to indicate that ^{36}Ar was trapped within the crystalline lattice of phengite during crystallization at UHP conditions at ~8 Ma.

Phengite ^{36}Ar concentrations range from 307 to 58×10^{-14} mol g^{-1}, whereas omphacite ^{36}Ar concentrations range from 41.45 to 3.57×10^{-14} mol g^{-1} (Table S2). These values are comparable with previously reported ^{36}Ar concentrations in antigorite (1.2×10^{-12} mol g^{-1}) and olivine enstatite (0.15×10^{-12} mol g^{-1}) (7). The measured ^{36}Ar concentrations for omphacite are similar to ^{36}Ar abundances for bulk mantle ($7.8 \pm 4.3 \times 10^{-14}$ mol g^{-1}) normalized to the mass of the silicate Earth (44). It is important to note that ^{36}Ar concentrations are not homogenously distributed within the coesite eclogite, with phengite outgassing more ^{36}Ar than omphacite. The same is true for ^{20}Ne concentrations, with phengite outgassing 74–31×10^{-14} mol g^{-1} and omphacite outgassing 13–1.4×10^{-14} mol g^{-1} (Table S2). We infer that the measured variations in ^{36}Ar and ^{20}Ne in omphacite and phengite from the coesite eclogite are related to differences in their ionic porosity (i.e., percentage void space in unit cell), with micas having a higher anionic porosity than pyroxenes (45). However, we also note that, based on studies of Ar diffusion in enstatite (8), it may not be possible to fully outgas Ar in pyroxene during laboratory heating, and hence, the lower abundances measured for omphacite may also reflect a higher Ar retentivity relative to phengite.

The combined dataset indicates that both atmospheric Ar and Ne were trapped in phengite and omphacite during crystallization and that $^{40}Ar/^{39}Ar$ phengite ages reliably record the timing of UHP metamorphism. None of these plots alone (Figs. 2, 3, 4, 5, and 6) permit full assessment of the composition of nonradiogenic Ar and Ne trapped in phengite and omphacite from the coesite eclogite analyzed. However, together, they clearly reveal the timing and composition of trapped Ar and Ne in hydrous K-bearing minerals, such as phengite. Results call for a reevaluation of phengite Ar data in other high-pressure and UHP terranes, especially in those studies in which $^{40}Ar/^{39}Ar$ phengite ages have been interpreted as geologically meaningless (46, 47).

Recycling of Atmospheric Ar and Ne in Forearcs

The first discovery of UHP conditions recorded in serpentinite shows subduction to pressures exceeding 30 kbar (48) and confirms that serpentinite subduction is a mechanism that can deliver high abundances of noble gas and chlorine to the mantle (7). High noble gas concentrations have been documented in seafloor and forearc serpentinites and their olivine enstatite dehydration residues, with ^{36}Ar concentrations that vary over three orders of magnitude (7, 13), but these lithologies have been difficult to date directly (49). The data presented here together with concordant phengite, zircon, and garnet ages and thermobarometric constraints on coesite eclogite indicate that atmospheric Ar and Ne were trapped in phengite and omphacite at mantle depths at ~8 Ma. These data document both the depth and timing of entrapment of atmospheric Ar and Ne in minerals (phengite and omphacite) crystallized during UHP metamorphism and returned to the surface. We infer that atmospheric Ar and Ne are present during subsolidus crystallization in the forearcs of subduction zones and that exhumed UHP terranes may represent a significant, heretofore unrecognized source of recycled atmospheric noble gases returned from mantle depths to the Earth's surface. Low geothermal gradients within forearcs favor both the retention of trapped Ar and Ne and also, the preservation of coesite (22) during UHP rock exhumation to the surface.

Geophysical evidence has recently provided direct evidence that links exhumed UHP rocks at the surface and subducted continental crust at depth (50). There is presently insufficient data to calculate the flux of atmospheric noble gases returned to the surface by exhumed UHP rocks. To determine the flux of atmospheric noble gases (e.g., the flow of Ar per unit time through a specified area) in minerals exhumed from mantle depths requires knowledge of when minerals formed during crystallization at mantle depths and their noble gas concentrations. Although we are presently unable to quantify the flux of atmospheric noble gases recycled in forearcs, given the history of subduction on Earth and the >20 UHP terranes recognized to date (17), the flux may be significant. Furthermore, the discovery of chromitites, rapidly exhumed from the mantle transition zone

(51), suggests that UHP minerals likely preserve additional clues related to exchange of material, including noble gases, from the deep Earth to the surface.

Methods

Mineral separates were prepared using standard heavy-liquid and magnetic separatory techniques. Phengite and omphacite separates were irradiated for 30 min in the Cadmium-Lined In-Core Irradiation Tube of the 1 MW TRIGA Reactor at the Oregon State University Radiation Center. All argon and neon analyses were performed in the Syracuse University Noble Gas Isotopic Research Laboratory. Irradiated samples are indicated in tables and plots; all other data were collected on aliquots of natural (unirradiated) material. Details of noble gas analyses can be found in *SI Noble Gas Procedures*.

ACKNOWLEDGMENTS. The authors thank the reviewers and the editor for constructive reviews. We thank E. B. Watson, P. G. Fitzgerald, M. G. Malusà, and J. B. Thomas for discussions. We also thank J. P. Catalano for assistance in the noble gas laboratory. This research was supported by National Science Foundation Geoscience Directorate, Division of Earth Sciences Continental Dynamics Program Grant EAR 0709054, National Aeronautics and Space Administration Astrobiology Grant NNA09DA80A, and Syracuse University.

1. Peacock SA (1990) Fluid processes in subduction zones. *Science* 248(4953):329–337.
2. Hacker BR, Abers GA, Peacock SA (2003) Subduction factory 1. Theoretical mineralogy, densities, seismic wave speeds, and water contents. *J Geophys Res* 108(B1): 2029–2055.
3. Kerrick DM, Connolly JAD (2001) Metamorphic devolatilization of subducted marine sediments and the transport of volatiles into the Earth's mantle. *Nature* 411(6835): 293–296.
4. Green HW, 2nd, Chen WP, Brudzinski MR (2010) Seismic evidence of negligible water carried below 400-km depth in subducting lithosphere. *Nature* 467(7317):828–831.
5. Hilton DR, Fischer TP, Marty B (2002) Noble gases and volatile recycling in subduction zones. *Noble Gases in Geochemistry and Cosmochemistry*, eds Porcelli D, Ballentine CJ, Wieler R (Mineralogical Society of America, Washington, DC), Vol 47, pp 319–370.
6. Burnard P, Zimmermann L, Sano Y (2013) *The Noble Gases as Geochemical Tracers: History and Background. The Noble Gases as Geochemical Tracers, Advances in Isotope Geochemistry*, ed Burnard P (Springer, Berlin), pp 1–15.
7. Kendrick MA, Scambelluri M, Honda M, Phillips D (2011) High abundances of noble gas and chlorine delivered to the mantle by serpentinite subduction. *Nat Geosci* 4(11): 807–812.
8. Watson EB, Thomas JB, Cherniak DJ (2007) 40Ar retention in the terrestrial planets. *Nature* 449(7160):299–304.
9. Harrison D, Burnard PG, Trieloff M, Turner G (2003) Resolving atmospheric contaminants in mantle noble gas analyses. *Geochem Geophys Geosyst* 4(3):1023–1040.
10. Ozima M, Zahnle K (1993) Mantle degassing and atmospheric evolution:noble gas view. *Geochem J* 27(4-5):185–200.
11. Raquin A, Moreira M (2009) Atmospheric 38Ar/36Ar in the mantle:implications for the nature of the terrestrial parent bodies. *Earth Planet Sci Lett* 287(3-4):551–558.
12. Matsumoto T, Chen Y, Matsuda J (2001) Concomitant occurrence of primordial and recycled noble gases in the Earth's mantle. *Earth Planet Sci Lett* 185(1-2):35–47.
13. Kendrick MA, et al. (2013) Subduction zone fluxes of halogens and noble gases in seafloor and forearc serpentinites. *Earth Planet Sci Lett* 365:86–96.
14. Kerrick D (2002) Geology. Serpentinite seduction. *Science* 298(5597):1344–1345.
15. Sumino H, et al. (2010) Seawater-derived noble gases and halogens preserved in exhumed mantle wedge peridotite. *Earth Planet Sci Lett* 294(1-2):163–172.
16. Mizukami T, Wallis S (2005) Structural and petrological constraints on the tectonic evolution of the garnet-lherzolite facies Higashi-akaishi peridotite body, Sanbagawa belt, SW Japan. *Tectonics*, 10.1029/2004TC001733.
17. Gillotti JA (2013) The realm of ultrahigh-pressure metamorphism. *Elements (Queb)* 9(4):255–260.
18. Malusà MG, et al. (2015) Contrasting styles of (U)HP rock exhumation along the Cenozoic Adria-Europe plate boundary (Western Alps, Calabria, Corsica). *Geochem Geophys Geosyst* 16:1786–1824.
19. Scambelluri M, Philippot P (2001) Deep fluids in subduction zones. *Lithos* 55(1-4): 213–227.
20. McDougall I, Harrison TM (1999) Geochronology and *T*hermochronology by the 40Ar/39Ar *M*ethod (Oxford Univ Press, New York), 2nd Ed.
21. Sumino H, Dobrzhinetskaya LF, Burgess R, Kagi H (2011) Deep-mantle-derived noble gases in metamorphic diamonds from Kokchetav massif, Kazakhstan. *Earth Planet Sci Lett* 307(3-4):439–449.
22. Baldwin SL, Webb LE, Monteleone BD (2008) Late Miocene coesite-eclogite exhumed in the Woodlark Rift. *Geology* 36(9):735–738.
23. Davies HL, Warren RG (1988) Origin of eclogite-bearing, domed, layered metamorphic complexes ("core complexes") in the D'Entrecasteaux Islands, Papua New Guinea. *Tectonics* 7(1):1–21.
24. Hill EJ (1994) Geometry and kinematics of shear zones formed during continental extension in eastern Papua New Guinea. *J Struct Geol* 16(8):1093–1105.
25. Little TA, et al. (2011) Diapiric Exhumation of Earth's youngest (UHP) eclogites in the gneiss domes of the D'Entrecasteaux Islands, Papua New Guinea. *Tectonophysics*, 10.1016/j.tecto.2011.06.006.
26. Davies HL, Warren RG (1992) Eclogites of the D'Entrecasteaux Islands. *Contrib Mineral Petrol* 112(4):463–474.
27. Baldwin SL, Lister GS, Hill EJ, Foster DA, McDougall I (1993) Thermochronologic constraints on the tectonic evolution of active metamorphic core complexes, D'Entrecasteaux Islands, Papua New Guinea. *Tectonics* 12(3):611–628.
28. Brownlee SJ, et al. (2011) Predicted velocity and density structure of the exhuming Papua New Guinea ultrahigh-pressure terrane. *J Geophys Res* 116(B8):B08206.
29. Zirakparvar NA, Baldwin SL, Vervoort JD (2012) The origin and geochemical evolution of the Woodlark Rift of Papua New Guinea. *Gondwana Res* 23(3):931–943.
30. Baldwin SL, Fitzgerald PG, Webb LE (2012) Tectonics of the New Guinea region. *Annu Rev Earth Planet Sci* 40:495–520.
31. Monteleone BD, et al. (2007) Late Miocene-Pliocene eclogite-facies metamorphism, D'Entrecastreaux Islands, SE Papua New Guinea. *J Metamorph Geol* 25(2):245–265.
32. Zirakparvar NA, Baldwin SL, Vervoort JD (2011) Lu-Hf garnet geochronology applied to plate boundary zones: Insights from the (U)HP terrane exhumed within the Woodlark Rift. *Earth Planet Sci Lett* 309(1-2):56–66.
33. Baldwin SL, et al. (2004) Pliocene eclogite exhumation at plate tectonic rates in eastern Papua New Guinea. *Nature* 431(7006):263–267.
34. Lee J-Y, Marti K, Severinghaus JP, Kawamura K, Yoo H-S, Lee JB, Kim JS (2006) A redetermination of the isotopic abundances of atmospheric Ar. *Geochim Cosmochim Acta* 70(17):4507–4512.
35. Scaillet S (1998) K-Ar (40Ar/39Ar) geochronology of ultrahigh pressure rocks. *When Continents Collide: Geodynamics and Geochemistry of Ultrahigh-Pressure Rocks*, eds Hacker BR, Liou JG (Kluwer, Dordrecht, The Netherlands), Vol 10, pp 161–201.
36. Schmidt MW, Vielzeuf D, Auzanneau E (2004) Melting and dissolution of subducting crust at high pressures: The key role of white mica. *Earth Planet Sci Lett* 228(1-2):65–84.
37. Kendrick MA, Burnard P (2013) Noble gases and halogens in fluid inclusions: A journey through the Earth's crust. *The Noble Gases as Geochemical Tracers*, ed Burnard P (Springer, Berlin), pp 319–369.
38. Fleet ME (2003) *Sheet Silicates: Micas* (The Geological Society, London), 2nd Ed.
39. Sano Y, Marty B, Burnard P (2013) Noble gases in the atmosphere. *The Noble Gases As Geochemical Tracers*, ed Burnard P (Springer, Berlin), pp 17–31.
40. Moreira M (2013) Noble gas constraints on the origin and evolution of Earth's volatiles. *Geochem Perspect* 2(2):403.
41. Moreira MA, Kurz MD (2013) Noble gases as tracers of mantle processes and magmatic degassing. *The Noble Gases as Geochemical Tracers*, ed Burnard P (Springer, Berlin), pp 371–391.
42. Moreira M, Allegre CJ (1998) Helium-neon systematics and the structure of the mantle. *Chem Geol* 147(1-2):53–59.
43. Ozima M, Podosek FA (2002) *Noble Gas Geochemistry* (Cambridge Univ Press, Cambridge, United Kingdom), 2nd Ed.
44. Marty B (2012) The origins and concentrations of water, carbon, nitrogen and noble gases on Earth. *Earth Planet Sci Lett* 313-314:56–66.
45. Dowty E (1980) Crystal-chemical factors affecting the mobility of ions in minerals. *Am Mineral* 65(1-2):174–182.
46. Li S, et al. (2011) Thermochronological constraints on two-stage extrusion of HP/UHP terranes in the Dabie–Sulu orogen, east-central China. *Tectonophysics* 504(1-4):25–42.
47. Warren CJ, Kelley SP, Sherlock SC, McDonald CS (2012) Metamorphic rocks seek meaningful cooling rate: Interpreting 40Ar/39Ar ages in an exhumed ultra-high pressure terrane. *Lithos* 155:30–48.
48. Shen T, et al. (2015) UHP metamorphism documented in Ti-chondrodite and Ti-clinohumite-bearing serpentinized ultramafic rocks from Chinese southwestern Tianshan. *J Petrol* 56(7):1425–1458.
49. Rubatto D, Scambelluri M (2003) U-Pb dating of magmatic zircon and metamorphic baddeleyite in the Ligurian eclogites (Voltri Massif, Western Alps). *Contrib Mineral Petrol* 146(3):341–355.
50. Zhao L, et al. (2015) First seismic evidence for continental subduction beneath the Western Alps. *Geology* 43(9):815–818.
51. McGowan NM, et al. (2015) Tibetan chromitites: Excavating the slab graveyard. *Geology* 43(2):179–182.
52. Hacker BR (2006) Pressures and temperatures of ultrahigh-pressure metamorphism: Implications for UHP tectonics and H2O in subducting slabs. *Int Geol Rev* 48(12): 1053–1066.
53. Turrin BD, Donnelly-Nolan JM, Hearn BC (1994) $^{40}Ar/^{39}Ar$ ages from the rhyolite of Alder Creek, California: Age of the Cobb Mountain normal-polarity subchron revisited. *Geology* 22(3):251–254.
54. Steiger RH, Jager E (1977) Subcomission on geochronology: Convention on the use of decay constants in geo- and cosmochronology. *Earth Planet Sci Lett* 36(3):359–362.